

A radiometric normalization method of Controlling No-Changed Set (CNCS) for diverse landcover using multi-sensor data

LiTing Huang¹, WeiLi Jiao^{2,*}, TengFei Long², ChuanLi Kang¹

¹ College of Geomatics and Geoinformation, Guilin University of Technology, Guilin, China

² Institute of Remote Sensing and Digital Earth Chinese Academy of Sciences, Beijing, China

KEY WORDS: Multi-sensor, Radiometric Normalization, Automatic Scattergram-controlled Regression, Multivariate Alteration Detection, No-Changed Set

ABSTRACT:

The accurate acquisition of land surface reflectance (SR) data determines the accuracy of ground objects recognition, classification and land surface parameter inversion using remote sensing data, which is the basis of remote sensing data application. In this study, a Control No-Changed Set (CNCS) radiometric normalization method is proposed to realize spectral information transformation of multi-sensor data, which is based on the Iteratively Reweighted Multivariate Alteration Detection (IR-MAD), and includes automatic selection and step-by-step optimization of no-change pixels. The No-Changed set (NC) is obtained by selecting the original no-change pixels between the target image and the reference image according to the linear relationship. In the obtained original no-change regions, IR-MAD rules with iterative control are used to fix the final no-change pixels, after regression modeling and calculation, the normalized images are obtained. The method is tested on multi-images from multi-sensors in three groups of experiments (GF-1 WFV and Landsat-8 OLI, GF-1 PMS and Sentinel-2 MSI, and Landsat-8 OLI and Sentinel-2 MSI) with different landcover areas. The results of radiometric normalization are evaluated qualitatively and quantitatively. The data of the three groups of experiments have a high correlation (correlation coefficient r values > 0.85), indicating that they can be used together as complementary data. The Root Mean Squared Error (RMSE) values calculate from the NC between the reference and normalized target images are much smaller than those between the reference and original target images. The radiometric colour composition effects, and the typical ground objects spectral reflective curves of the reference and normalized target images are very similar after radiometric normalization. These results indicate that the CNCS method considers the linear relationship of the no-change pixels and is effective, stable, and can be used to improve the consistency of SR of multi-images from multi-sensors.

1. INTRODUCTION

The accurate acquisition of land surface reflectance (SR) data determines the accuracy of ground objects recognition (Zhang et al., 2015), land cover classification (Friedl et al., 2010) and land surface parameter inversion (Nazeer et al., 2017) using remote sensing data, which is the basis of remote sensing data application. At the same time, the variety of remote sensing satellites is increasing, which makes the remote sensing data resources multi-source. However, the response to the ground reflection spectrum of different satellite sensors is inconsistent, resulting in differences in SR acquired by different satellites. Therefore, it is necessary to improve the consistency between data by spectral radiometric normalization before multi-source data joint application. There are many methods about radiometric normalization at present: Dark Set-Bright Set Normalization (DB) (Hall et al., 1991), Pseudo-invariant Feature (PIF) (Schott et al., 1988), Automatic Scattergram-controlled Regression (ASCR) (Elvidge et al., 1995), and Iteratively Reweighted MAD (IR-MAD) (Canty and Nielsen, 2008), etc. Previous studies have evaluated the various radiometric normalization methods over different types and times of land covers images. For example, Lin et al. (2015) utilized principal component analysis to determine the major axis of the bitemporal image scatterplot and to extract PIFs with the determined major axis. In Zhong et al. (2016), a hierarchical

regression method is proposed to reduce the radiometric differences for multitemporal images, which consists of extraction of the pseudo-invariant features (PIFs) and optimization of normalization parameters. Zhou et al. (2016) presented the utilization of normalized difference water index (NDWI) to select the original PIFs, and statistical rules with iterative control were used to fix the final PIFs. Recently, Syariz et al. (2019) proposed a constrained orthogonal regression, a common radiometric level located between bitemporal images is selected as the reference, which enforces pixel spectral signatures to be as consistent as possible during radiometric normalization while band regression quality is preserved. But these radiometric normalization methods do not involve the physical mechanism of remote sensing, and do not fully consider the influence factors such as atmosphere, so it is often impossible to obtain high-precision SR, which is not conducive to quantitative parameter inversion of multi-source remote sensing data.

In this study, a method is proposed to normalize radiometric using IR-MAD to Control No-Changed Set (CNCS). This normalization method is based on the regression modelling using invariant pixels known as No-Changed set (NC) from the target image and the reference image, which is a better approach than using global or half of the image pixels for radiometric normalization (Yang et al., 2000). To select the NC, the

* Corresponding author
E-mail address: jiaowl@radi.ac.cn (WeiLi Jiao)

preliminarily no-change pixels are selected through scattergrams used in automatic scattergram-controlled regression, which is the conventional linear regression method. The final no-change pixels are acquired through the regularized IR-MAD rule on the preliminarily selected NC, then using orthogonal regression, and a normalized target image is obtained. The objectives of this study are:

1. Reduce the complexity of atmospheric correction. For the target image with unsatisfactory atmospheric correction effect, the SR can be improved by reference image with better accuracy.
2. Radiometric normalization is used to further improve the consistency of radiometric information from multi-sensors remote sensing images.

In this paper, GF-1 Wide Field of View (WFV) and Landsat-8 Operational Land Imager (OLI), GF-1 Panchromatic Multispectral Sensor (PMS) and Sentinel-2 Multi-Spectral Instrument (MSI), Landsat-8 OLI and Sentinel-2 MSI are taken as examples to carry out three groups of experiments.

The remainder of this paper is organized as follows: Section 2 describes the proposed method. Section 3 shows the experimental data. Section 4 presents the experimental results, and Section 5 provides the conclusions and future works.

2. METHODOLOGY

This study proposes a CNCS radiometric normalization method based on the Iteratively Reweighted Multivariate Alteration Detection (IR-MAD). This method does not require the image to have both dark and bright features, and can eliminate the influence of large sample noise on the radiometric correction results. The proposed method consists of four main steps, namely, preliminary extract NC, final screening NC, orthogonal regression, and radiometry transformation, which will be described in Sections 2.1, 2.2, and 2.3, respectively. Among them, Section 2.2 is the focus of this study.

2.1 Preliminary Extract NC

General relative radiometric normalization methods assume that radiometric relationships between the corresponding bands of target image and reference image are linear, and rectify the target image to a reference image through a linear transformation (Biday et al., 2010). The common form for linear radiometric normalization is given by

$$y_i = ax_i + b \quad (1)$$

where y_i is the digital number (DN) of band i in the reference image; x_i is the DN of band i in the target image; and a , b are normalization coefficients for band i .

First, the no-change pixels are selected from the reference image and the target image, and then the normalization coefficients are calculated, and finally radiometry transformation.

Elivdige et al. (1995) proposed the ASCR in relative radiometric normalization. The ASCR procedure locates the centers for land and water data clusters using the near-infrared (NIR) target image data versus reference image data scattergrams to establish

an initial regression line, and then determine the NC. However, not all images have land and water conditions at the same time. Therefore, the CNCS differs from the ASCR method in that the former does not need the land and water data clusters on the scattergrams to determine the NC. It is on the scattergrams of the red and NIR bands, the orthogonal regression method (which is introduced in 2.3) is used to determine the initial regression baseline, and then further filters the no-change pixels to solve the NC. Solving the initial regression line is shown in Figure 1.

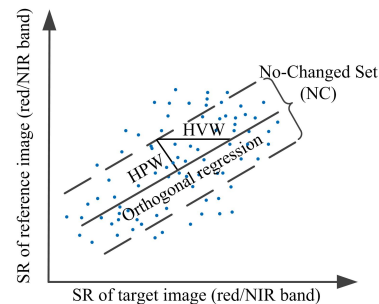


Figure 1. Determine the No-Change set (NC) from the scattergrams

HVW in the Fig. 2 is the restriction condition of NC, controlled by HPW, and HPW is the vertical width of one side of the NC. HPW, HVW and NC have the following relationship (Elvidge et al., 1995):

$$HVW_{NC} = \sqrt{1 + a^2} * HPW_{NC} \quad (2)$$

$$NC = (X, Y) : |y_1 - b_1 - a_1 x_1| \leq HVW_{NC1} \ \& \ |y_2 - b_2 - a_2 x_2| \leq HVW_{NC2} \quad (3)$$

Where a is the slope of the initially estimated axis determined by orthogonal regression. Once the HVW is determined, the initial NC can be determined by Equation (3), where y_1 and y_2 are SR values of red band and NIR band of the reference image, respectively; x_1 and x_2 are SR values of red band and NIR band of the target image, respectively; and a_i and b_i are coefficients determined by orthogonal regression.

The NC determined by the linear transformation roughly represents a "pseudo-invariant" pixel set, that is, a pixel whose radiation characteristics hardly change (Seo et al., 2017).

2.2 Final screening NC

The quality of the no-change pixels affect the result of radiometric normalization, and further optimization of the no-change pixel is required in the NC. Use the following rules to find sample data that can be used for regression (Canty and Nielsen, 2008): Set the initial weight of each pixel as 1, calculate the mean vector and the variance matrix in each iteration, and calculate each MAD variate with the method of canonical correlation analysis; the weight of the pixels are updated according to the newly calculated MAD variates, and the weight range is [0,1]; the no-change pixel has a large weight, and after several iterations, the weight of each pixel tends to be stable; by comparing the weight with the threshold, it is possible to determine whether a pixel is a no-change pixel or not.

The formulas for updating weights are:

$$\sigma_{MAD_i}^2 = \gamma_i = 2(1 - \rho_{N-i+1}) \quad (4)$$

$$Z = \sum_{i=1}^N \frac{(MAD_i)^2}{\gamma_i} \in \chi^2(N) \quad (5)$$

$$P_r(\text{no change}) = 1 - P_{\chi^2, N}(Z) \quad (6)$$

Where γ_i is the variance of band i , and Z is a random variate introduced by iterative assignment, which represents the sum of the standard MAD variates squares, obeys the chi-square distribution with degree of freedom N (band number), and is weighted by chi-square distribution probability density function. $P_r(\text{no change})$ represents the iteration weight, and a fixed threshold t can be set (for example, $t=0.95$ can be set to obtain a good result). When $P_r(\text{no change}) > t$, the pixel can be assigned a label “no-change”. This is described in detail in Canty and Nielsen (2008).

There are many (correlated) variables during the iteration, the solutions to the coupled generalized eigenvalue problems may become unstable due to (near) singular variance covariance matrices causing small changes in the data to lead to dramatically different solutions. Therefore, Nielsen(2007) added regularization (also known as penalization) in the iterative process to avoid the weight generated being too large, and affect the judgment of the no-change pixels. In this study, regularization parameter is also added when solving the covariance matrices:

$$Var_{11} = \sum_{11} + \lambda_1 \Omega_1 \quad (7)$$

$$Var_{22} = \sum_{22} + \lambda_2 \Omega_2 \quad (8)$$

Where λ_i is a regularization parameter, whose range is $[0 \sim 1]$, and Ω_i is a diagonal matrix of $N \times N$.

2.3 orthogonal regression, and radiometry transformation

Orthogonal regression method based on geometric distance is adopted (Leng et al., 1988). Suppose there are k data points $P_i(x_i, y_i), i=1 \dots k$ in the two-dimensional plane, the regression analysis is to obtain a straight line L as shown in formula (1) $y_i = ax_i + b$ by some criterion. Minimize $D = \sum_{i=1}^k d(P_i, L)$, where $d(P_i, L)$ is the geometric distance from point P_i to L . In orthogonal regression, a can be estimated according to

$$a = \frac{(S_{yy}^2 - S_{xx}^2) + \sqrt{(S_{yy}^2 - S_{xx}^2)^2 + 4S_{xy}^2}}{2S_{xy}} \quad (9)$$

$$S_{xx}^2 = \frac{1}{n} \sum_{i=1}^n (x_i - \bar{x})^2 \quad (10)$$

$$S_{yy}^2 = \frac{1}{n} \sum_{i=1}^n (y_i - \bar{y})^2 \quad (11)$$

$$S_{xy} = \frac{1}{n} \sum_{i=1}^n (x_i - \bar{x})(y_i - \bar{y}) \quad (12)$$

Where \bar{x} and \bar{y} is the mean of x , y , respectively. And b can be calculated according to a , that is $b = \bar{y} - a\bar{x}$.

After obtaining the NC in Section 2.2, the regression equation can be established in the NC for relative radiometric normalization from the above equations.

3. DATA AND PRE-PROCESSING

Sentinel-2 Level-2A are bottom of the atmosphere (BOA) reflectance products, which can be produced by Sen2cor, a processor for Level-2A data released by European Space Agency (ESA)(Louis et al., 2016). It is also available through the URL <https://scihub.copernicus.eu/dhus/#/home>, and can be downloaded the Level-2A data in China region since December 2018.

Landsat-8 OLI Level-2 Surface Reflectance data are generated from the Land Surface Reflectance Code (LaSRC). LaSRC makes use of the coastal aerosol band to perform aerosol inversion tests, uses auxiliary climate data from MODIS and uses a unique radiative transfer model (Badawi et al., 2019). LaSRC is regarded as the most accurate for Landsat-8 OLI atmospheric correction, and Level-2 data can be freely downloaded at <https://earthexplorer.usgs.gov/>.

GF-1 has no relevant SR products released. The DN images are downloaded from China Center for Resource Satellite Data and Applications (<http://www.cresda.com/CN/>). DN images need to be pre-processed with atmospheric correction to obtain SR products. In this study, atmospheric correction of GF-1 images are performed based on ARCSI (Atmospheric and Radiometric Correction of Satellite Imagery) (Clewley et al., 2014).

As the resolution of the three satellites are inconsistent, resampling processing is needed before radiometric normalization to make the resolution of target image consistent with that of reference image.

In the experiments, three satellite images that contain various landscapes are used for relative radiometric normalization in four bands of blue, green, red and NIR, which verified the feasibility and performance of the proposed method. The properties of satellites are tabulated in Table 1.

Table 1. Overview of the main parameters of the multiple sensors

Sensor	Spectral range (μm)	Resolution (m)	Revisit periods(day)
GF-1 WFV	Band1(blue): 0.45-0.52	16	2
	Band2(green): 0.52-0.59		
	Band3(red): 0.63-0.69		
	Band4(NIR): 0.77-0.89		
GF-1 PMS	Band1(blue): 0.45-0.52	8	3~5
	Band2(green): 0.52-0.59		
	Band3(red): 0.63-0.69		
	Band4(NIR): 0.77-0.89		
Landsat-8 OLI	Band2(blue): 0.45-0.51	30	16
	Band3(green): 0.53-0.59		
	Band4(red): 0.64-0.67		
	Band5(NIR): 0.85-0.88		
	Band2(blue): 0.46-0.52		
Sentinel-2 MSI	Band3(green): 0.54-0.58	10	10
	Band4(red): 0.65-0.68		
	Band8(NIR): 0.79-0.90		

The experiments are divided into three groups, Dataset 1, Dataset 2 and Dataset 3, and all groups included three sets of experiments. Landsat-8 OLI is selected as the reference image in Dataset 1 and 3, and Dataset 2 selects the Sentinel-2 MSI as the reference image. The study area images should be selected on the same date as much as possible to ensure that the remote

sensing images are less affected by the atmosphere. However, because different satellites have different revisit periods and swaths, it is difficult to obtain different satellite images of the same date and transit at the same time. In this study, the date difference between the target image and the reference image is no more than seven days. Three study areas, comprising various landscapes, including desert, agricultural crop, and urban area, are selected as shown in Table 2-4 for method evaluation.

Table 2. GF-1 WFV and Landsat-8 OLI study areas


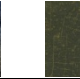
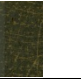
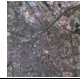


	WFV4	OLI	WFV3	OLI	WFV2	OLI
Dataset 1						
Path, row	137, 032		123, 037		122, 033	
Acquisitions date	20180512,		20180409,		20180924,	
	20180512		20180408		20180924	
Image size	500×500		500×500		500×500	

Table 3. GF-1 PMS and Sentinel-2 MSI study areas





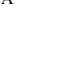







	PMS1	S2B	PMS1	S2B	PMS1	S2A
Dataset 2						
Path, row	021, 090		599, 105		052, 081	
Acquisitions date	20181213,		20181128,		20180807,	
	20181216		20181128		20180807	
Image size	500×500		500×500		500×500	

Table 4. Sentinel-2 MSI and Landsat-8 OLI study areas

	S2B	OLI	S2A	OLI	S2B	OLI
Dataset 3						
Path, row	126, 029		122, 038		123, 032	
Acquisitions date	20181225,		20180417,		20181118,	
	20181230		20180420		20181121	
Image size	500×500		500×500		500×500	

4. EXPERIMENTAL RESULTS AND DISCUSSION

4.1 The process of selecting NC

Taking the reflectance of the target image band as the X-axis and that of the reference image band as the Y-axis, the red and NIR band of the target image and the reference image respectively generate a scattergram to determine the initial regression line and extract NC. Taking Dataset 1 as an example, the NC scatterplots from step-by-step selection process for Dataset 1 are displayed in Figure 2. The black dots in the figure represent all the pixels of the image, the blue dots are the initially extracted NC, the yellow dots are the last extracted NC, the green lines represent the initial regression line, and the red lines represent the final fitted line. It should be noted that the SR values of the experimental images here are all scaled by 10,000 times.

These scattergrams have some common characteristics: The no-change pixels gradually converge, and the number of points in the last scatter diagram decreases, and are distributed along a straight line; the slope of the principal axis varies slightly from the second to the third time; the variation range of scattergrams gradually decrease, and all points are slightly evenly distributed.

These characteristics indicate the effectiveness and stability of the method in the selection of NC.

Table 5. Quantitative validation of desert study area

Type	Group	Band	Slope (a)	Intercept (b)	RMSE		r
					Before	After	
Desert	Dataset 1 (WFV4 and OLI)	blue	0.496	-582.591	2902.016	9.711	0.980
		green	0.515	-259.834	2689.402	13.485	0.981
		red	0.558	-374.429	2887.102	13.289	0.990
		NIR	0.553	-193.524	2843.463	14.231	0.992
	Dataset 2 (PMS1 and S2B)	blue	4.405	-1562.813	437.6416	15.325	0.994
		green	4.161	-1792.187	898.047	20.603	0.995
		red	3.882	-1917.920	1391.316	30.328	0.995
		NIR	3.629	-1672.024	1699.054	41.131	0.994
	Dataset 3 (S2B and OLI)	blue	0.691	421.698	133.165	11.753	0.976
		green	0.850	396.980	167.842	12.717	0.993
		red	0.843	323.132	78.175	15.392	0.996
		NIR	0.846	345.674	174.273	16.008	0.997

Table 6. Quantitative validation of agricultural crop study area

Type	Group	Band	Slope (a)	Intercept (b)	RMSE		r
					Before	After	
Agricultural crop	Dataset 1 (WFV3 and OLI)	blue	1.765	-843.482	356.120	20.992	0.857
		green	1.272	-419.039	219.996	13.022	0.963
		red	1.177	-209.879	141.956	11.596	0.972
		NIR	1.601	-1723.864	624.098	42.485	0.989
	Dataset 2 (PMS1 and S2B)	blue	0.676	-667.739	1292.754	12.433	0.998
		green	0.683	-511.636	1203.032	14.155	0.998
		red	0.719	-564.539	1153.685	18.082	0.999
		NIR	0.754	-893.043	2348.282	23.918	0.999
	Dataset 3 (S2A and OLI)	blue	0.832	-3.841	105.102	10.733	0.995
		green	0.732	195.700	56.784	11.026	0.995
		red	0.724	209.097	92.115	17.290	0.997
		NIR	0.683	856.039	309.409	66.33	0.990

Table 7. Quantitative validation of urban area study area

Type	Group	Band	Slope (a)	Intercept (b)	RMSE		r
					Before	After	
Urban area	Dataset 1 (WFV2 and OLI)	blue	0.881	-12.823	103.002	40.559	0.982
		green	0.985	-74.506	90.613	36.662	0.989
		red	1.086	-132.531	65.014	25.453	0.996
		NIR	1.374	-665.786	242.263	35.079	0.998
	Dataset 2 (PMS1 and S2B)	blue	0.789	-988.000	1557.496	24.153	0.998
		green	0.705	-585.814	1362.544	25.686	0.997
		red	0.707	-508.159	1295.387	14.796	0.999
		NIR	0.740	-763.092	1728.091	34.370	0.997
	Dataset 3 (S2B and OLI)	blue	0.533	336.150	196.223	29.447	0.974
		green	0.636	351.022	230.765	21.171	0.994
		red	0.669	327.021	221.335	20.915	0.996
		NIR	0.735	350.426	234.809	29.657	0.997

4.2 Qualitative and quantitative parameters statistical analysis

To measure the overall differences, two-thirds of the sample points in the NC are regression fitted, and the rest are used as validation data to quantify the results of the radiometric normalization. Table 5-7 list the normalization coefficients for each band for the three group experiments. All of the experiments are quantitatively evaluated using the root-mean-square error (RMSE) and correlation coefficient (r). RMSE is defined as $RMSE = \sqrt{\frac{1}{N} \sum_{i=1}^N (y'_k - y_k)^2}$, where y'_k is the SR value of target image band k after radiometric normalization, y_k is the SR value of reference image band k , and N is the number of samples. And r is defined as

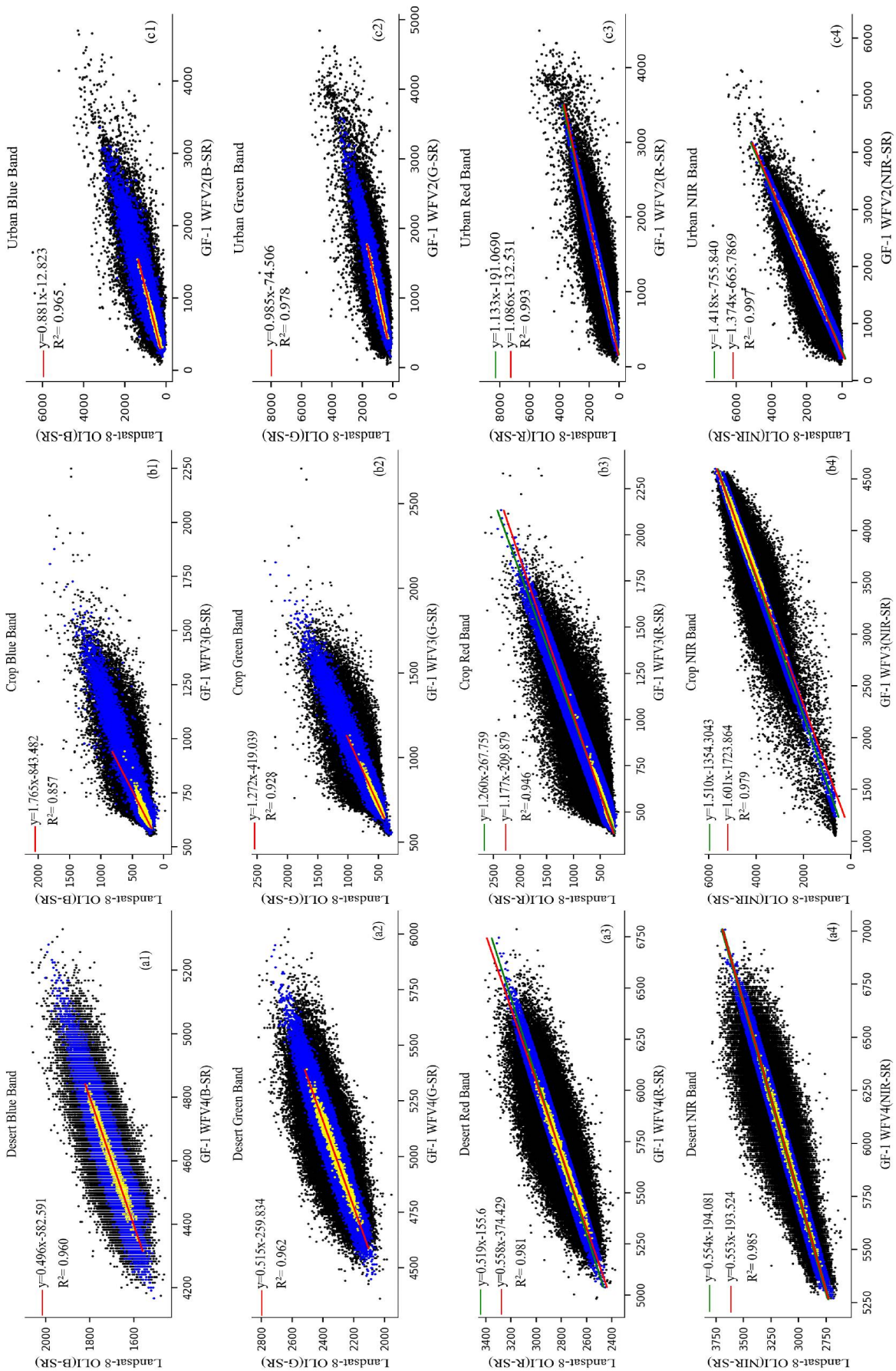


Figure 2. Gf-1 WFV and landsat-8 OLI NC selection process

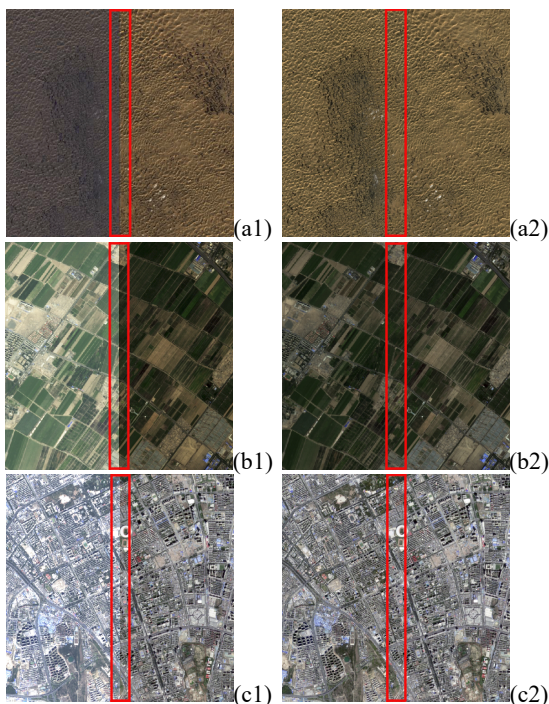


Figure 3. Radiometric normalization results of Dataset 2. First column: original target image (left) and reference image (right). Second column: normalization result image of proposed method (left) and reference image (c2) (right).

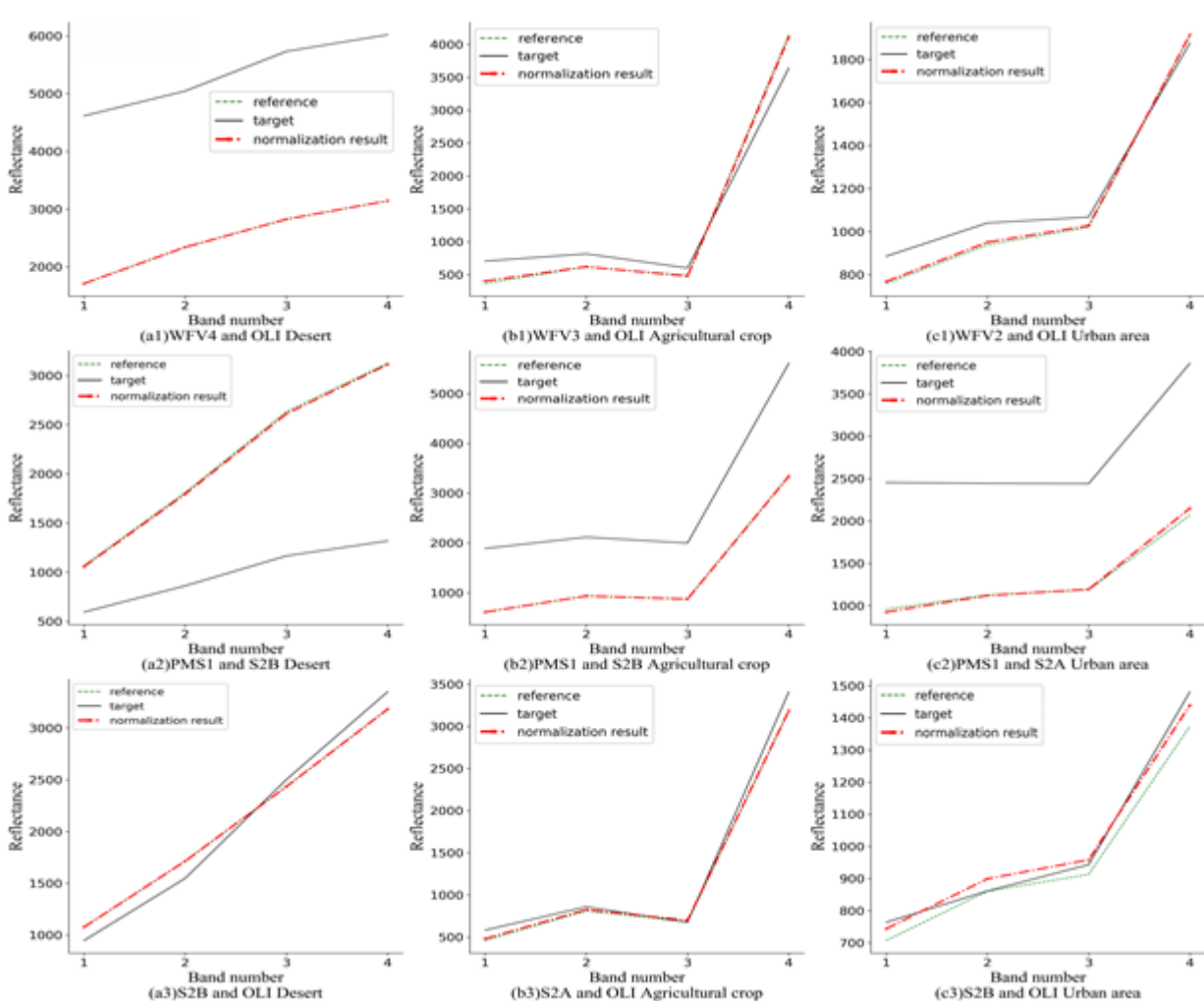


Figure 4. Comparison of spectral reflective curves of the ground objects before and after normalization

$$r(y'_k, y_k) = \frac{Cov(y'_k, y_k)}{\sqrt{Var[y'_k]Var[y_k]}}. \text{ From Table 5-7, it can be seen}$$

that the RMSE of the normalized image is smaller than that before radiometric normalization, and the r values of the bands exceed 0.857, and the highest r is 0.999, which shows that CNCS method can effectively reduce the radiometric differences between the target image and the reference image, and the correlation between the target and reference data is closer after radiometric normalization.

In addition, from the normalization coefficients, we can see the difference of SR products of different satellite sensors. In the desert area, the slope coefficients of GF-1 WFV and Landsat-8 are much less than 1, and the slope coefficients of GF-1 PMS and Sentinel-2B are much greater than 1, indicating that the ARCSI atmospheric correction method is not effective enough in desert area. This is due to the ARCSI method uses the dark dense vegetation approach to retrieve aerosols for atmospheric correction, while there is a lack of sufficient vegetation in the desert area.

The result of radiometric normalization is qualitatively evaluated by visual comparison. The normalized image is compared with the reference image, if the color and brightness of the two images are very similar, the normalization effect is better. Only the visual comparison results of Dataset 2 are listed here. The image colour composition effects of the normalized target images are more similar to those of the reference images than to those of the original target images. The radiometric differences between the original target and reference images are greatly reduced. These results are observed for all landcover areas from Figure 3.

Due to the radiometric distortion and the characteristics of different sensors, the spectral reflective curve characteristics of the ground objects are very different. One of the purposes of CNCS is to eliminate or reduce these differences. The more similar the spectral reflective curves of the ground objects are, the closer the spectral characteristics of the ground objects are, and the variation of the spectral curve can indicate the effect of relative radiometric normalization to a certain extent. It can be seen from Figure 4 that the spectral reflective curve of the radiometric normalized image is closer to the reference image, indicating that the radiometric normalization is effective.

It can be seen from the above results that although the atmospheric correction effects of different satellite images are not the same, the CNCS relative radiometric normalization method can improve the SR accuracy of the target image based on the reference image with better atmospheric correction effect. The purpose of reducing the complexity of atmospheric correction and improving the radiation consistency of multi-source images is achieved.

5. CONCLUSIONS

A Control No-Changed Set (CNCS) radiometric normalization method is proposed. To validate the method under as many different conditions as possible, three groups of experiments with different landscape types are carried out. The results show that the NC selection method is consistently effective. The results of the three groups of experiments using the CNCS method are that: (1) The RMSE values calculated from the NC between the reference and normalized target images are much smaller than those between the reference and original target images, and the r values of each band are close to 1; (2)

Visually comparing the results, the differences in the image edge of different landscapes (desert, agricultural crop, and urban area) are significantly reduced, the colour composition effects of the images after radiometric normalization are very similar; (3) After radiometric normalization, the spectral reflective curves of the typical ground objects are close to the reference images, indicating that the radiometric normalization is effective.

The uncertainties in the results are primarily caused by two factors. First, the uncertainties may have been caused by image registration errors. The geometrical registration errors are nearly one or two pixels, which would cause a mismatch of the no-change pixels locations between the original target and reference images. Second, the spectral range differences and spectral response differences among multiple sensors will affect the result of atmospheric correction, resulting in differences of reflectivity of the same ground object on different images. In near future, the spectral range differences and spectral response differences among multi-sensor will be studied.

ACKNOWLEDGEMENTS

This work has been supported by the Strategic Priority Research Program of the Chinese Academy of Sciences (grant number XDA19090300), the National Natural Science Foundation of China (grant number 61731022), the National Key R&D Program of China (grant number 2016YFA0600302).

REFERENCES

- Badawi, M., Helder D., Leigh, L., Jing, X., 2019. Methods for Earth-Observing Satellite Surface Reflectance Validation. *Remote Sens.* 11(13): 1543.
- Biday, S.,G., Bhosle, U., 2010. Radiometric correction of multitemporal satellite imagery. *Journal of Computer Science.* 6(9): 940-949.
- Canty, M.J., Nielsen, A.A., 2008. Automatic radiometric normalization of multitemporal satellite imagery with the iteratively re-weighted MAD transformation. *Remote Sens. Environ.* 112(3): 1025-1036.
- Clewley, D., Bunting, P., Shepherd, J., Gillingham, S., Flood, N., Dymond, J., Lucas, R., Armston, J., Moghaddam, M., 2014. A Python-Based Open Source System for Geographic Object-Based Image Analysis (GEOBIA) Utilizing Raster Attribute Tables. *Remote Sensing.* 6: 6111-6135.
- Elvidge, C.D., Yuan, D., Weerackoon, R.D., Lunetta, R.S., 1995. Relative radiometric normalization of landsat Multispectral Scanner (MSS) data using an automatic scattergram-controlled regression. *Photogramm. Eng. Remote Sens.* 61(10): 1255-1260.
- Friedl, M.A., Sulla-Menashe, D., Tan, B., Schneider, A., Ramankutty, N., Sibley, A., Huang, X., 2010. MODIS Collection 5 global land cover: Algorithm refinements and characterization of new datasets. *Remote Sens. Environ.* 114, 168-182.
- Hall, F.G., Strelbel, D.E., Nickeson, J.E., Goetz, S.J., 1991. Radiometric rectification: Toward a common radiometric response among multitemporal, multisensor images. *Remote Sens. Environ.* 35(1), 11-27.

Leng, L., Zhang, T.Y., Kleinman, L., Zhu, W., 2007. Ordinary Least Square Regression, Orthogonal Regression, Geometric Mean Regression and their Applications in Aerosol Science. *Journal of Physics Conference Series*. 78(1): 1-5.

Lin, C.H., Lin, B.Y., Lee, K.Y., Chen, Y.C., 2015. Radiometric normalization and cloud detection of optical satellite images using invariant pixels. *ISPRS J. Photogramm. Remote Sens.* 106, 107-117.

Louis, J., Debaecker, V., Pflug, B., Main-Knorn, M., Bieniarz, J., Müller-Wilm, U., Cadau, E., Gascon, F., 2016. Sentinel-2 Sen2cor: L2A processor for users. *ESA Living Planet Symposium*. 6(9): 1027-1036.

Nazeer, M.; Wong, M.S.; Nichol, J.E., 2017. A new approach for the estimation of phytoplankton cell counts associated with algal blooms. *Sci. Total Environ.* 590, 125-138.

Nielsen, A.A., 2007. The regularized iteratively reweighted MAD method for change detection in multi- and hyperspectral data. *IEEE Transactions on Image Processing*. 16(2): 463-478.

Schott, J.R., Salvaggio, C., Volchok W J. 1988. Radiometric scene normalization using pseudoinvariant features. *Remote Sens. Environ.* 26(1): 1-16.

Seo, D.K., Yong, H.K., Yang, D.E., Wan, Y.P., 2017. Generation of radiometric, phenological normalized image based on random forest regression for change detection. *Remote Sensing*. 9(11): 1-21.

Syariz, M.A., Lin, B.Y., Denaro L.G., Jaelani, L.M., Nguyen, M.V., Lin, C.H., 2019. Spectral-consistent relative radiometric normalization for multitemporal Landsat 8 imagery. *Int. J. Remote Sens.* 147:56-64.

Yang, X.J., Lo, C.P., 2000. Relative radiometric normalization performance for change detection from multi-date satellite images. *Photogramm. Eng. Remote Sens.* 66(8): 967-980.

Zhang, R., Qu, J.J., Liu, Y., Hao, X., Huang, C., Zhan, X., 2015. Detection of burned areas from mega-fires using daily and historical MODIS surface reflectance. *Int. J. Remote Sens.* 36, 1167-1187.

Zhong, C., Xu, Q., Li, B., 2016. Relative radiometric normalization for multitemporal remote sensing images by hierarchical regression. *IEEE Geosci. Remote Sens. Lett.* 13 (2), 217-221.

Zhou, H., Liu, S., He, J., Wen, Q., Song, L., Ma, Y., 2016. A new model for the automatic relative radiometric normalization of multiple images with pseudo-invariant features. *Int. J. Remote Sens.* 37 (19), 4554-4573.

Revised September 2019